Pharm Res (2011) 28:2311–2326
DOI 10.1007/s11095-011-0461-2

RESEARCH PAPER

Compositional Analysis of Low Quantities of Phase Separation in Hot-Melt-Extruded Solid Dispersions: A Combined Atomic Force Microscopy, Photothermal Fourier-Transform Infrared Microspectroscopy, and Localised Thermal Analysis Approach

Sheng Qi • Peter Belton • Kathrin Nollenberger • Andreas Gryczke • Duncan Q. M. Craig

Received: 3 February 2011 / Accepted: 26 April 2011 / Published online: 24 May 2011

ABSTRACT

Purpose To characterise phase separations in aged hot-melt-extruded solid dispersions at a micron to submicron scale.

Methods Hot-melt-extruded felodipine and Eudragit® E PO systems at a range of compositions were studied after a standard period of aging to allow phase separation to occur. The samples were characterised using combined nano-thermal analysis, photothermal FTIR microspectroscopy coupled with pulsed force mode AFM as a novel characterisation approach.

Result Crystalline felodipine presents in all formulations with drug loadings from 10–70% (w/w). In formulations with high drug loadings (50 and 70%), amorphous felodipine co-exists with crystalline forms, and higher drug concentration is observed in the centre compared to the outer surface of the extrudates. Drug crystal dimensions in extrudates with low drug loadings (10–30%) are small, in the micron to submicron range. We propose that uneven drug distribution is principally caused by processing-associated factors such as expansion of extrudates during extrusion.

Conclusions We have demonstrated that the novel combined approach allows site-specific characterisation of the extruded systems and that drug distribution may be uneven across the extrudates, with concomitant implications for understanding stability and drug release behaviour.

KEY WORDS hot-melt-extruded solid dispersion · phase separation · photothermal FTIR microspectroscopy · pulsed force mode atomic force microscopy · supersaturation

INTRODUCTION

Hot melt extrusion (HME) has been used for polymer processing for decades and is a single-step solvent-free process of reshaping molten/softened polymer by the application of heat and mechanical stress. The approach has become increasingly adopted into the pharmaceutical arena for the preparation of solid dispersion formulations (1–3). In common with other solid dispersion systems prepared by fusion and solvent evaporation (i.e. spray drying, film casting), phase separation of the drug and polymer in HME formulations is a key issue, either on initial production or on storage. Phase separation is often present as crystalline or amorphous drug domains with dimensions varying from few hundred nm to few microns. On extrusion, the drug and polymer may form an intimate (molecular level) mix due to the application of a combination of heat and shear pressure. However, if the amount of drug in the polymer exceeds its equilibrium solid solubility, the drug either separates or else may be in a thermodynamically unstable supersaturated state after extrusion (4,5), leading to long-term stability issues such as drug crystallisation. In most cases, phase separation is undesirable and is considered to lead to potentially significant

Electronic Supplementary Material The online version of this article (doi:10.1007/s11095-011-0461-2) contains supplementary material, which is available to authorized users.

S. Qi (✉) · D. Q. M. Craig
School of Pharmacy, University of East Anglia
Norwich, Norfolk, NR4 7TJ, UK
e-mail: sheng.qi@uea.ac.uk

P. Belton
School of Chemistry, University of East Anglia
Norwich, Norfolk, NR4 7TJ, UK

K. Nollenberger · A. Gryczke
Evonik Röhm GmbH
Kirschenallee
64293 Darmstadt, Germany

reductions in the therapeutic effect of a formulation because of the slower dissolution of the drug crystals compared to the molecularly dispersed form. Therefore, controlling phase separation is of critical importance in solid dispersion pharmaceutical formulations in general and, on the basis of current interest, HME formulations in particular.

On storage, the dimensions and quantity of the separated phases may increase as a function of time in a manner which is not yet fully understood. At the early stage of phase separation, low numbers of sub-micron-sized separated phase domains may be present in the formulation. This generates difficulties with regard to the detection of the phase separation due to the quantities and dimensions involved being below the detection limits of many commercially available analytical tools, such as differential scanning calorimetry (DSC) and powder X-ray diffraction (PXRD). These characterisation tools can provide little information on the distribution of the separated phases. However, if the phase separation is not discovered at an early stage, further growth of the phase-separated domains is highly likely, leading to significant product performance issues with high associated costs; hence, early detection is considered highly desirable. Additionally, for some conventional analytical methods, it is necessary to grind the original solid dosage forms to produce a powder for analysis; this pulverisation process may well compromise the initial physical form of the system.

The main focus of this study is to develop new characterisation approaches to identify low levels of phase separation of small dimensions in intact HME samples. Here we use felodipine, a calcium channel blocker used in the treatment of cardiovascular disease, as a model poorly water-soluble drug. Eudragit® E PO was used as the model polymer for hot melt extrusion; this material is a methacrylate copolymer. Our previous study estimated the equilibrium solid solubility of felodipine in Eudragit® E PO below 10% (w/w) (6). No phase separation was tested in the freshly prepared samples with drug loading up to 50% (w/w) (6). However, after aging (2 months, 20°C/40% RH), phase separation was observed in all formulations with drug loadings from 10% to 70% (w/w). Therefore, in this study, only aged hot-melt-extruded formulations were investigated. Early identification of phase separation using conventional macroscopic analytical methods, such as DSC, has been shown to be difficult due to the low quantity of separated material, and, when using imaging methods such as SEM, there are difficulties associated with identifying the physical and chemical nature of the observed structures (6). This study proposes a new way of addressing this problem by combining pulsed force mode atomic force microscopy (PFM-AFM) with the newly developed technique of localised nano-thermal analysis (LTA) and photothermal Fourier-Transfer Infrared (PT-FTIR) microspectroscopy (7–9). A previous study demonstrated the potential of micro-thermal analysis in the characterisation of hot-melt-extruded formulations (10). In the current study, the working resolution of probe-based thermal analysis was further improved by using nano-thermal probes (7), while the use of PT-FTIR microspectroscopy presents a new method of chemically identifying the drug distribution profile across the hot melt extrudates. This approach interfaces heated AFM tip with FTIR spectroscopy in that the thermal fluctuations associated with the applied IR beam are detected using the (Wollaston) thermal probe in passive (measurement) mode to produce an interferogram which is then used to generate an IR spectrum via Fourier transformation (8,9,11). Here we introduce its use as a means of studying drug distribution in polymers for the first time.

MATERIALS AND METHODS

Felodipine form I (mp: 145°C) and Eudragit® E PO were supplied from Zhejiang Yiyuan, China and Evonik Röhm GmbH, (Darmstadt, Germany), respectively. Amorphous felodipine was prepared by quench cooling from the melt. The crystalline felodipine and Eudragit® E PO compressed tablets for the PFM-AFM study were prepared using a 13 mm evacuable IR pellet press (Specac, Kent, UK) with a 5 ton compression for 30 s.

Hot Melt Extrusion

Hot melt extrusion was carried out using a co-rotating twin screw Haake Minilab extruder (Thermo Fisher, Karlsruhe, Germany). For the samples containing Eudragit® E PO and felodipine, the temperature was set at 160°C, the screw speed was 100 rpm, and the mixture was manually fed into the extruder. The samples were pressed through a single orifice die and collected on a cooled conveyer belt as strands. The torque was as follows: for 10% (w/w) felodipine 23Ncm, for 20% (w/w) felodipine 26Ncm, for 30% (w/w) felodipine 24Ncm, for 50% (w/w) 22Ncm and for 70% (w/w) felodipine 20Ncm. The aged samples were characterised after 2 months storage at 20°C/40%RH.

ATR-FTIR Spectroscopy

The IR spectra of the samples were collected using an FTIR spectrometer (IFS66/S model from Bruker Optics limited, Coventry, UK) with a mercury/cadmium/telluride detector. The HME strands were directly placed on a single-reflection diamond ATR (attenuated total reflectance)

accessory (Specac, Orpington, UK); this modification allows the extrudate to be examined as is without the need for grinding. Thirty two scans were acquired for each sample with a resolution of 2 cm^{-1}. All measurements on the side surface and the cross-section centre surface of the cylinder-shaped extrudates were preformed triplicate. The spectra of crystalline felodipine and Eudragit® E PO were taken as references. The Fourier Self-Deconvolution (FSD) process was performed using OMINC (Thermo Nicolet Corporation, Madison, USA), and the FSD parameters used are with bandwidth of 75.9 and enhancement of 1.5.

Pulsed Force Mode AFM (PFM-AFM)

PFM-AFM imaging was performed using a Veeco Explorer (Veeco, CA, USA) coupled with a Witec PFM module (Witec, Ulm, Germany). Thermal nanoprobes (AN nanoprobes) (Anasys Instruments, Santa Barbara, USA) were used for the analysis; these probes have a spring constant of 0.7–2 N/m. They were used for the PFM-AFM and local thermal analysis experiments since they can be used for contact, noncontact, and intermittent contact modes. However, the values of the pull-off force on identical samples may vary with individual probes; hence, these values are not absolute. In addition, the pull-off force values are expressed in nA in order to minimise the difference caused by the changing of the force constant value of the individual probe. Only two probes were used throughout the entire study, and the two probes had similar force constants. A scanning speed of 0.5 Hz was used at a resolution of 200 lines. The probe was subjected to a modulation of 500 Hz and approximate amplitude of 110 nm. Each image was obtained over an approximately 20-min period.

Localised Thermal Analysis (LTA) Using Nano-Thermal Probes

LTA was performed using a Nano Thermal Analyzer (Anasys Instruments, Santa Barbara, USA) with a Veeco diCaliber scanning probe microscope head (Veeco, CA, USA) and a thermal nanoprobe (AN nanoprobes) (Anasys Instruments, Santa Barbara, USA). Samples were fixed to the magnetic stub using double-sided tape and mounted onto an X-Y translating microscope stage. The instrument was calibrated for temperature and displacement. Poly(e-caprolactone) (PCL with T_m at 60°C), polyethylene (PE with T_m at 130°C) and poly(ethylene terephthalate) (PET with T_m at 238°C) (Anasys Instruments, Santa Barbara, USA) were used as calibrants for temperature calibration; the room temperature 'kick-in point' was used as the other known temperature point for a four points calibration (8,11). In this work, LTA was performed using a net 'force' of 10 ± 1 nA and a heating rate of 10°C/s from 25°C to 180°C on the surface of the extrudates. A 10×10 μm^2 AFM image was generated in the first instance. The thermal nanoprobe was brought to selected locations on the AFM image, and LTA measurements were performed at each point. Three to five locations were selected and tested on the surface of each sample.

Photothermal Fourier-Transform Infrared (PT-FTIR) Microspectroscopy

PT-FTIR microspectroscopy analysis was performed by interfacing (using a dedicated optical interface) a Thermomicroscopes Explorer AFM (Veeco, CA, USA) equipped with a Wollaston wire thermal probe (Veeco, CA, USA) and a FTIR spectrometer (IFS66/S model from Bruker Optics limited, Coventry, UK). Ten different locations on the side and cross-section surface of the HME samples were selected. After tip contact, 56 scans of each tested point were acquired at a resolution of 8 cm^{-1}.

RESULTS

Phase separation has previously been indicated in the aged HME formulations with 10–70% drug loadings using heat capacity measurements and NMR relaxometry (6). However, in the earlier study, it proved very difficult to identify the physical state of felodipine using conventional thermal methods due to the extremely similar glass transition temperatures of the amorphous drug and the polymer as well as the absence of discernible drug melting in most aged formulations. It was also difficult or even impossible (for formulations with low drug loadings) to evaluate the drug distribution across the extrudates using these analytical methods. In the current study, therefore, we use ATR-FTIR spectroscopy to identify the physical form of the crystalline drug in the aged formulations. PFM-AFM was then employed to map the phase separation at a submicron scale. The localised characterisation and identification of the separate phases was further investigated using LTA and PT-FTIR microspectroscopy. We discuss each of these approaches in turn below.

Macroscopic Analysis of Phase Separation and Drug Distribution of the Aged HME Formulations Using ATR-FTIR Spectroscopy

Raw Materials

ATR-FTIR spectroscopy has been used to identify the physical state of the drug in solid dispersions and to

estimate the distribution of the drug in hot-melt-extruded formulations (10). The partial ATR-FTIR spectra of the crystalline felodipine polymorphic form I, amorphous felodipine (prepared by supercooling of felodipine melt) and Eudragit® E PO powders are shown in Fig. 1. It was extremely difficult to achieve pure felodipine polymorphic form II (12). As it is not the main focus of this study, the reference IR data of the form II was obtained from literature (12–15). The N-H region of the raw materials was first examined (circa 3300–3400 cm^{-1}), as the polymer has no peak in this region, while felodipine has an N-H functional group that acts as a hydrogen donor and acceptor. This group is therefore capable of forming inter- and intra-molecular hydrogen bonds with function groups such as carbonyl within or between the drug molecules and, potentially, between the drug and the polymer molecules (13,15). The N-H stretching appears at 3369 cm^{-1} for crystalline felodipine form I and at 3336 cm^{-1} for felodipine polymorphic form II (12).

In felodipine form I, H-bonding only exists between two felodipine molecules, whereas each felodipine molecule can form H-bonds with two other felodipine molecules in the polymorphic form II crystal structure (see Supplementary Material). The weak H-bonding in the crystalline form I is believed to be partially caused by the shielding effect of the methyl groups in the dihydropyridine ring (12). The red shift of the N-H stretching from 3369 cm^{-1} (form I) to 3336 cm^{-1} (form II) is attributed to the enhanced hydrogen bonding between the N-H and C=O groups (12). Similar to form II, the amorphous felodipine prepared by supercooling of the felodipine melt shows N-H stretching at 3339 cm^{-1} with broadened peak width. This is in good agreement with published data (12,13,15). This indicates that the H-bonding between the N-H and C=O groups in the amorphous felodipine is stronger than the ones in the crystalline felodipine form I. A shoulder peak at 3416 cm^{-1}, which is also observed in the spectrum of the quench cooled amorphous felodipine, has been reported to be associated with a free N-H moiety (non H-bonding) (13,15).

In the 1600–1800 cm^{-1} region, the polymer and drug, both containing C=O groups, and molecular interaction such as H-bonding can cause shifts of the C=O stretching. Therefore, it is important to obtain clear understanding of the spectra of the raw materials and identify influencing factors of the shifts of the C=O groups in both the drug and the polymer molecules. There are distinguishable C=O stretching bands at 1687 cm^{-1} and 1725 cm^{-1} related to crystalline felodipine form I and Eudragit® E PO, respectively. The 1687 cm^{-1} peak is noted to be asymmetric in shape for felodipine form I (Fig. 1). After Fourier self-deconvolution (FSD), which is a process used to separate overlapped IR peaks, a 1697 cm^{-1} peak (non-H-bonded C=O group) can be seen clearly separated from the 1687 cm^{-1} peak; this result is again in good agreement with the literature (12,15). In the spectra of amorphous felodipine, the 1687 cm^{-1} shifts to 1677 cm^{-1} (H-bonded

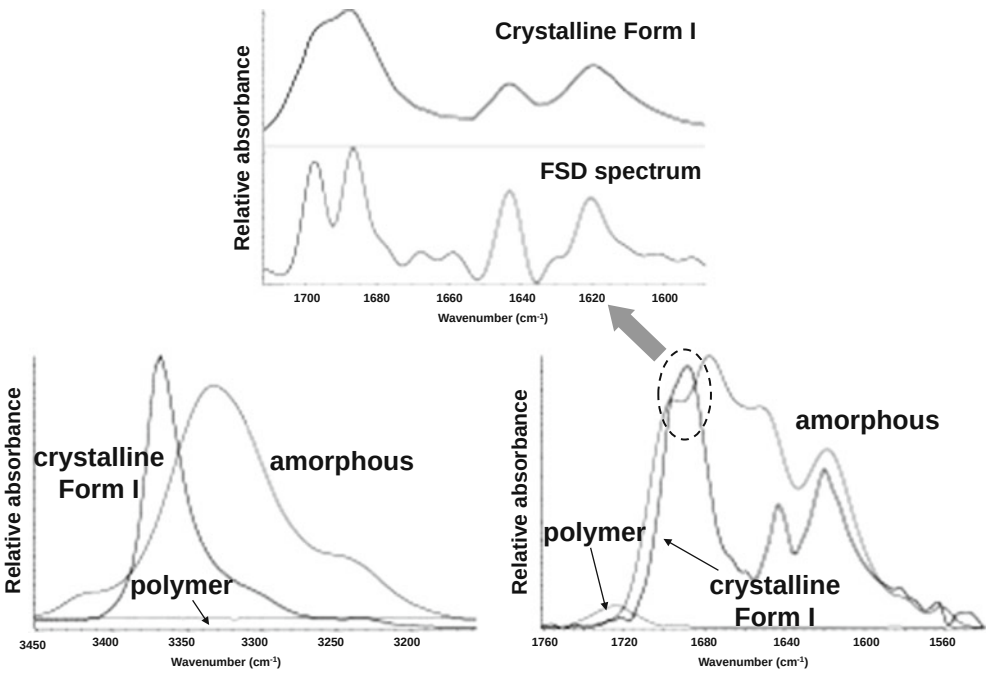

Fig. 1 Partial ATR-FTIR spectra of the crystalline, amorphous felodipine and Eudragit® E PO powders with a Fourier Self-Deconvolution (FSD) spectrum of the 1780–1580 cm^{-1} region of the crystalline feldoipine form I.

C=O group) with a shoulder peak at 1697 cm^{-1}. This shift indicates the increased inter- and intra-molecular H-bonding between the N-H and C=O groups in the amorphous felodipine. A similar red shift of the C=O stretching to 1684 cm^{-1} is also reported in the IR spectrum of felodipine form II (14). This confirms again that the amorphous and polymorphic form II felodipine both have stronger drug-drug H-bonding compared to crystalline felodipine form I. In this study, both N-H (3339 cm^{-1} and 3416 cm^{-1}–amorphous form; 3369 cm^{-1}–crystalline form I; 3336 cm^{-1}–crystalline form II) and C=O (1677 cm^{-1} and 1697 cm^{-1}–amorphous form; 1687 $cm^{-1}$and 1697 cm^{-1}–crystalline form I; 1684 cm^{-1}–crystalline form II) regions discussed above are therefore used to provide information on the identification of the physical states of the drug in the formulations and the interactions between felodipine and Eudragit® E PO.

Aged HME Solid Dispersions

In our previous study, the heat capacity and NMR relaxometry measurements indicated the coexistence of low quantity crystalline and amorphous felodipine in the aged HME formulations (10). However, it was inconclusive in terms of the crystalline drug distribution across the extrudates and the polymorphic form of felodipine in the formulations. In this study, the surface and the cross-section of the aged extrudates with different drug loadings were examined using ATR-FTIR spectroscopy. It is first noted that the N-H regions of the formulations with drug loadings up to 30% show no significant difference between the surface and the cross-sectional spectra (see Supplementary Material). N-H stretching is observed at 3369 cm^{-1} for these formulations, which is consistent with the presence of the crystalline felodipine form I. A weak peak at 3421 cm^{-1} indicates the presence of small quantity of non-H-bonded felodipine, possibly in the form of molecular dispersion with the polymer. The relative intensity of this peak decreases dramatically with increasing the drug loading.

The N-H peaks of the aged formulations with low drug loadings are at 3369 cm^{-1}, indicating the presence of crystalline form I. However, the 3369 cm^{-1} peak shows broadening in the peak width in comparison to that of the pure crystalline felodipine form I. Similar changes in peak width were also observed in the milled felodipine, which is crystalline but with smaller particle size and more defects than the initial felodipine crystalline form I (see Supplementary Material) (16–19). Therefore, this peak broadening may be associated with the small particle size of the form I felodipine crystals in the extrudates. In the C=O regions of these three formulations with drug loading from 10–30% (w/w), it is noted that the C=O bands of the polymer show no shift compared to the polymer alone. This indicates that the N-H group in the felodipine molecule does not form strong H-bonding with the C=O group in the polymer. This may be attributed to the more rigid chain structure of Eudragit® E PO, in which the C=O group is hidden in the middle of the polymer side chain and less exposed to intermolecular interaction compared to other polymers, such as polyvinylpyrrolidone (PVP), which is well known to form strong H-bonding with felodipine (13,15,20–22). The lack of drug-polymer interaction may also contribute to the low solubility of the drug in the polymer (6). The only visible C=O bands of felodipine in the spectra of these three formulations is at 1697 cm^{-1} as a shoulder peak of the polymer C=O peak confirming the presence of felodipine polymorphic form I. The intensity of this drug-associated C=O peak gradually increases with increasing the drug loading. However, the second C=O stretching (either 1677 cm^{-1} or 1682 cm^{-1}) is absent in the formulations of 10–30% drug loadings. Combined with previous heat capacity study (6), it can be concluded that felodipine presents as crystalline form I and possibly molecular dispersion (without being strongly H-bonded to the polymer) in the aged formulations with 10–30% drug loadings.

In the surface spectra of the 50% drug-loaded formulation, a 1684 cm^{-1} shoulder peak of the main peak at 1697 cm^{-1} can be identified after FSD, indicating the presence of possibly felodipine crystalline forms I and II (Fig. 2). For the 1684 cm^{-1} peak, a shoulder peak at 1679 cm^{-1} is found in the cross-section spectra of the 50/50 formulations, indicating the presence of a significant amount of amorphous felodipine in the centre of the aged 50/50 extrudates. A shoulder peak at 3337 cm^{-1} of the 3369 cm^{-1} peak is observed after FSD for the surface spectra, indicating the presence of felodipine crystalline forms I and II. Thus, the crystalline forms I and II co-exist at the surface of the aged 50/50 extrudates, while the cross-sectional spectra suggest the co-existence of amorphous and crystalline form II. The possible mechanism of the difference in the crystalline behaviour on the surface and in the inner core of the extrudates is discussed in a later section of the paper. The surface spectra of the 70/30 formulation displays a broad N-H stretching, which is a contribution of the overlapping of two peaks at 3369 cm^{-1} and 3340 cm^{-1} confirmed by the FSD. This indicates that for the 70/30 formulation, there is a mixture of crystalline (possibly a mixture of forms I and II) and amorphous drug on the surface of the extrudates, while the N-H stretching shifts to 3339 cm^{-1} in the cross-section spectra of the 70/30 formulation. The 1678 cm^{-1} C=O peaks are seen in both surface and cross-section spectra of the 70/30 formulation, indicating the presence of amorphous felodipine across the aged 70/30 extrudates. The possible reason for the drug loading and location dependence of the physical states of the drug will be discussed later in this paper.

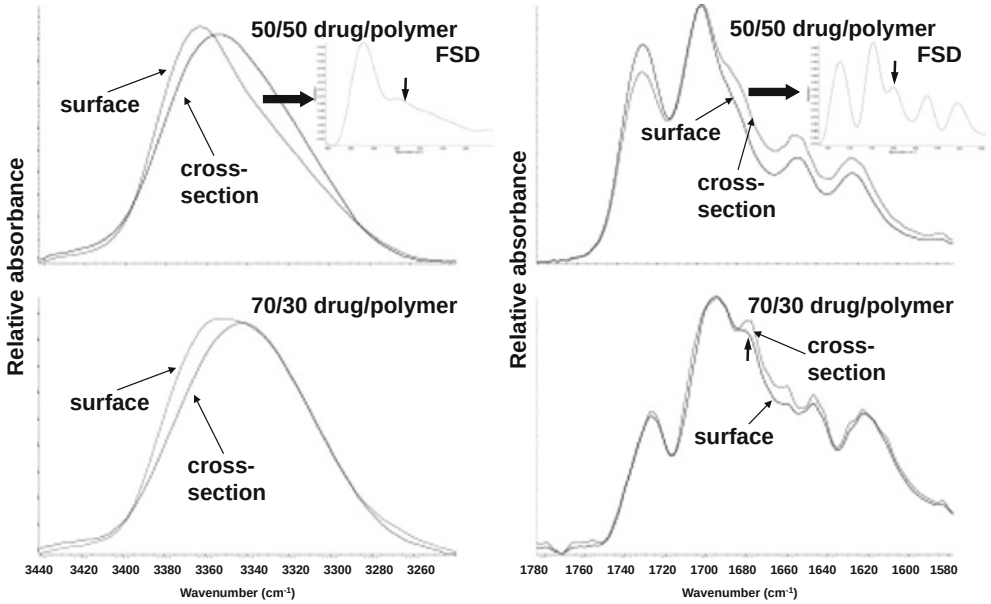

Fig. 2 Partial ATR-FTIR spectra of the surface and the cross-section of the aged 50/50 and 70/30 felodipine/ Eudragit® E PO HME extrudates in the regions of 3440–3240 cm^{-1} (*left panel*) and 1780–1580 cm^{-1}(*right panel*). (The axes of the FSD spectra of 50/50 extrudates are the same as the ATR-FTIR spectra.)

Ambient PFM-AFM Investigation of Phase Separation in the Aged HME Formulations

PFM-AFM is a particular mode of AFM involving the superimposition of a sinusoidal modulation to the z-axis piezo of the AFM tip during its movement. Following this modulation, the tip is pulled off from the surface after approaching, making contact, and indenting the surface at each sampling point (23–28). PFM-AFM allows for the measurements of the adhesion/stiffness of the sample surface via measuring the pull-off force of the tip across the samples surface. Therefore, the PFM-AFM technique has been successfully applied to measure the local stiffness and adhesion properties of a sample alongside the more usual topographic image (29–33).

Raw Materials

In order to establish the estimation on the adhesion forces of the raw materials individually, the pure crystalline felodipine form I and Eudragit® E PO in the form of compressed tablets were examined in the first instance. The histograms of the number of pixels as a function of pull-off force is an expression of the correlation between the colour contrast observed in the adhesion image and the surface property of the tested area. The histogram can in turn assist the estimation of the proportion of regions with different contrast, such as 'lighter' and 'darker' regions decoupled from the location of these regions in the images. In general, for a same drug its crystalline form tends to have lower adhesion ('darker' region) than its amorphous form ('lighter' region). For an amorphous polymer, if the test temperature is well below the T_g of the polymer, the adhesion of the polymer may not show significant difference compared to the crystalline material. This appears to be the case for the present study. The samples were tested at ambient conditions, while the glass transitions of the polymer and the amorphous drug are both at approximately 45°C, which is 25°C higher than the ambient temperature. As seen in Fig. 3, Gaussian distribution of the pull-off force of the pixels for the polymer (approximately 2.6 signal/volt as the peak value) and drug (approximately 4.1 signal/volt as the peak value) indicates the single component homogeneous surface for both. The crystalline felodipine is expected to have a narrow pull-off force distribution. However, it is noted that the distribution is broader for the crystalline felodipine compared to the pure polymer. This may be caused by the small amount of crystal defects generated on the surface of the tablet via compression process. Nevertheless, it can be concluded that the average pull-off force of the crystalline felodipine is slightly higher than Eudragit® E PO. Therefore, in the binary system of felodipine and the polymer, the drug-rich domains should appear as 'lighter' and the polymer rich domains being 'darker' in comparison. This information can be used for the interpretation of the histograms of felodipine/Eudragit® E PO formulations.

Aged HME Solid Dispersions with Low Drug Loadings

The surfaces of the aged extrudates were examined using PFM-AFM. As seen in Fig. 4, for the 10/90 and 20/80 HME extrudates, the topography and adhesion images

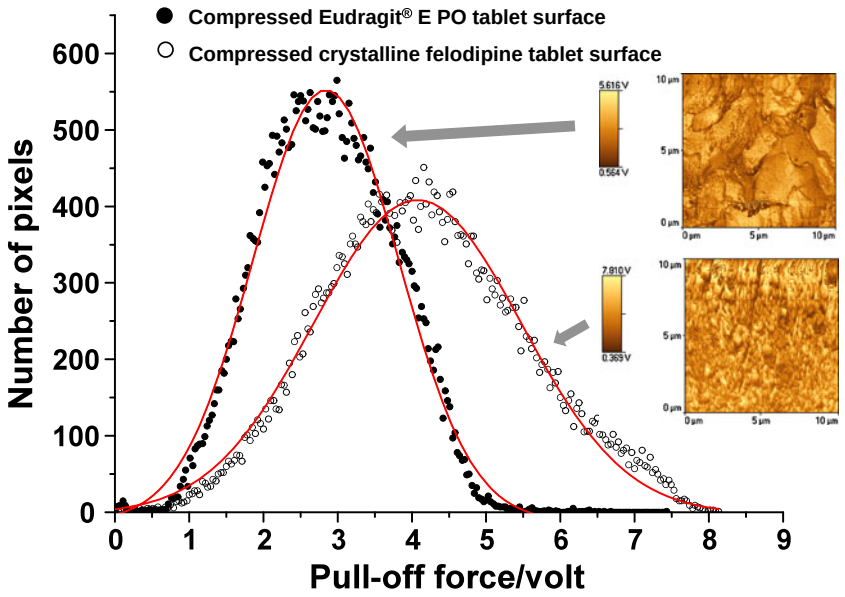

Fig. 3 The histograms of the compressed pure Eudragit® E PO and crystalline felodipine tablet surfaces with inserted adhesion images. Gaussian fitting is shown as solid line.

show significant differentiation in the contrast of the 'darker' and 'lighter' regions which do not directly correlate to the features observed in the topography images. Similar difference between the topography and adhesion images were reported in amorphous and crystalline lactose compressed tablets (33). This indicates that the roughness of the surface present in the topography images displays a low level of interference on the adhesion image. This is further confirmed by the linescan graphs from the topography and adhesion images of the formulations (see Supplementary Material). Therefore, it is reasonable to suggest that the contrast observed in the adhesion images largely reflects the

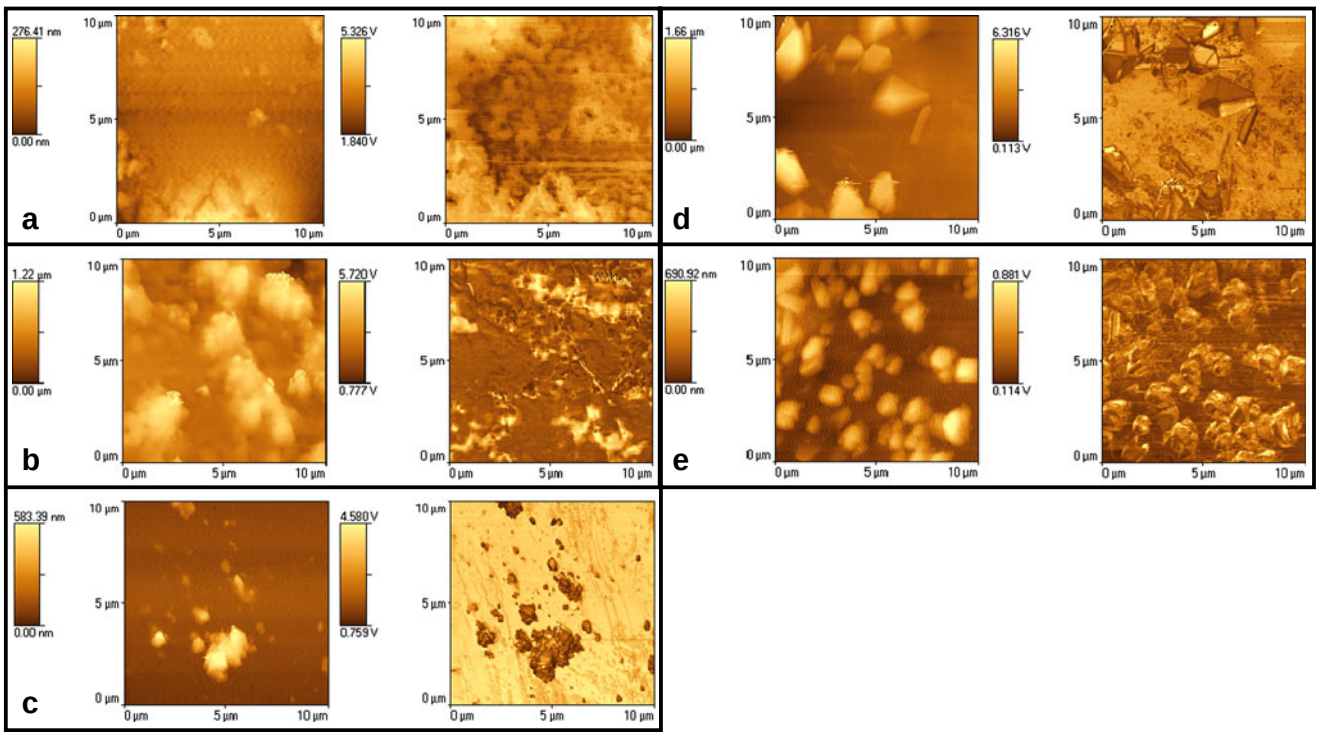

Fig. 4 PFM-AFM topography images (*left image in each panel*) and forward adhesion image (*right image in each panel*) of the surfaces of (**a**) 10/90; (**b**) 20/80; (**c**) 30/70; (**d**) 50/50; and (**e**) 70/30 aged felodipine/Eudragit® E PO HME extrudates.

difference in the pull-off force, which is an indication of the adhesive property of different regions. This can be demonstrated in detail using the histograms (see Supplementary Material).

As an example, the histogram of the adhesion image of the surface of a 20/80 extrudates shows a bimodal distribution of the pixels as demonstrated by the double Gaussian fitting of the peaks labelled as 1 and 2 in Fig. 5a. For peaks 1 and 2, the distribution of the pull-off force has the peak values approximately 2 and 4 signal/volt, respectively, which are close to the distribution of the pull-off force values of the pure polymer and pure crystalline drug. Lacking distinguishable crystalline particle feature in the topography image may imply that the crystalline drug is nano-crystals and observed as clusters in the image with shown spatial resolution (10×10 μm). This may also indicate that the sample mainly contains phase-separated polymer-rich and crystalline drug-rich domains. The number of pixels in the 'darker' region (represented by peak 1) is higher than the pixels in the 'lighter' region. The span of the peaks can be used as an indicator of the similarity of the pull-off force of the regions. The peak 2 associated with the 'lighter' region has broader distribution compared to the peak 1 associated with the 'darker' region, indicating that the 'lighter' regions are likely to be a mixture of polymer-rich domains with a wide range of drug concentrations. This is further demonstrated by the two selected areas (labelled as areas A and B) at the bottom of the image which contain pure 'darker' region and a region with a mixture of 'darker' and 'lighter' features but with higher contrast compared to the whole image. The histogram of the 'darker' area A shows a single narrow peak with low adhesive force, indicating the area only contains pure polymer. The histogram of the area B demonstrates a clearer separation of the distributions of the pixels in the 'darker' and 'lighter' regions compared to the histogram of the whole adhesion image. It is noted that three separated Gaussian distributions are required for an adequate fit to the data. The intermediate peak has been reported to be an artefact of tip penetration at the interface of the 'lighter' and 'darker' regions instead of a true separated phase (29).

Furthermore, the proportion of the integrated 'lighter' and 'darker' peak areas can be used as a rough quantitative estimation of drug content of the tested region. For 20/80 formulation (Fig. 5a), the proportion of the integrated peak areas associated with the 'lighter' and 'darker' regions in the histogram of the whole adhesion image is slightly higher than 20:80. This again implies that the 'lighter' regions are drug-rich polymer domains instead of pure drug domains. This proportion changed to approximately 50:50 in the histogram of the selected region B, indicating that within this local region there is higher drug content than the average drug content of the total tested surface. This result demonstrates the uneven distribution of the drug in the formulations with low drug contents at a micron to submicron scale.

Aged HME Solid Dispersions with High Drug Loadings

As the drug loading increases to 30% (w/w), particulate features with 0.5–1 μm in diameter can be seen in the topography images of the formulations (Fig. 4). The particle sizes increase to 1–3 μm in the 50/50 and 70/30 extrudates. The particle density also increases with increasing the drug loading. For the 30/70 formulation, clear contrast is observed in the adhesion image between the particle region and flat regions. However, surprisingly, the flat region appears to be lighter in colour than the particles in the adhesion image, indicating the flat region has higher adhesion than the particles. Multiple repeats provided similar images, indicating that this result is reproducible. This may be explained as the flat region is amorphous polymer-drug mixture and the presence of amorphous drug elevates the adhesiveness of the dispersion. This increases the 'brightness' of the flat region dramatically.

For the 50/50 and 70/30 formulations, 'lighter' and 'darker' regions co-exist on the particle surfaces in the adhesion images (Fig. 4). This may indicate that the particles are partially crystalline and partially amorphous or coated with the polymer outer layer. This is investigated further in detail using the histogram of the 50/50 formulation as an example. As seen in Fig. 5b, the histogram of the whole adhesion image (top left) displays a bimodal distribution of Gaussian fitting labelled as peak 1 and peak 2. After integration, the proportion of the two peak areas of the peaks 1 and 2 is nearly 50:50, which correlates well with the drug:polyer ratio of this formulation. The pixel distributions of the pull-off force of the peaks 1 and 2 have peak values approximately 2 and 3.8, respectively, close to the values for the pure polymer and largely crystalline drug. The peaks appear in a largely joint manner, correlating well with the low contrast observed between the 'lighter' and 'darker' regions in the adhesion image. In order to further confirm the physical form of the particles, a local area containing some flat region and half of a crystal-shaped particle was examined (highlighted at the top left corner of the adhesion image). The local histogram (top right) of this selected area shows clear separation of the two pull-off force distributions. As shown in the individual histograms, the flat and particle regions (bottom left and right) are associated with high (lighter in colour) and low (darker in colour) adhesion force, respectively. This indicates that the flat region is crystalline drug-rich domain, possibly mixture of drug nano-crystals and polymer, and the dark particle surface is likely to be coated with the polymer. This is in good agreement with the ATR-

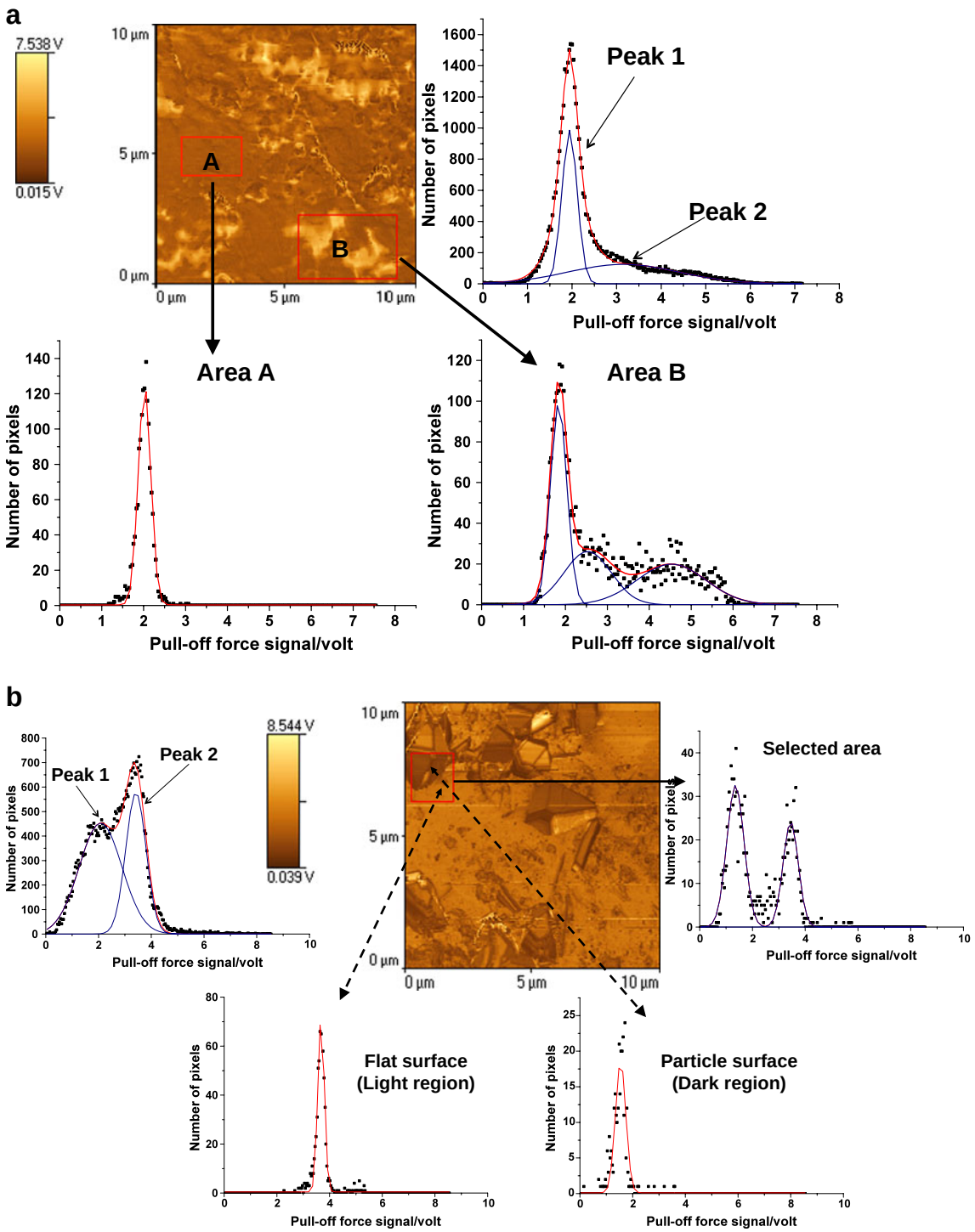

Fig. 5 (**a**) Whole (*top right plot*) and partial (*bottom plots*) histograms of an aged 20/80 felodipne/Eudragit® E PO extrudate surface, showing the pull-off force distribution at ambient temperature. The Gaussian curve fittings are shown as solid lines. (**b**) Whole (*top left plot*) and partial (*top right plot*) histograms of an aged 50/50 felodipne/Eudragit® E PO extrudate surface, showing the pull-off force distribution at ambient temperature. The pull-off force distributions of the 'darker' and 'lighter' regions in the highlighted area are shown in the bottom graphs. The Gaussian curve fittings are shown as solid lines.

FTIR spectroscopic results. An attempt was made to characterise the cross-section of the extrudates using PFM-AFM. However, due to the high friability, it was impossible to achieve relatively smooth cross-section surface for AFM scanning via any means of sectioning. Therefore, the detailed information on the cross-section of the sample

was only obtained using LTA and PT-FTIR microspectroscopy, since surface scanning using AFM probe is not essential for both techniques.

In summary, PFM-AFM has identified the phase separation presented in all formulations with micron to submicron dimension. In the low drug-loaded formulations, drug is likely to be mainly in nano-crystal form. With increasing the drug loading, the level of separation becomes more vigorous. Particulate-shaped separations with polymer coating were observed in the formulations with drug loadings at and above 30% (w/w).

Localised Identification of Phase Separation in the Aged HME Formulations

Local Thermal Analysis (LTA) of Phase Separation Using Nano-Thermal Probes

LTA has been used for the characterisation of multi-component pharmaceutical systems at a micron scale (6,7,33). The introduction of the new nano-thermal probes allows for the characterisation probing a submicron level (7). Furthermore, the use of the nano-thermal probes in principle can increase the spatial resolution and reduce the thermal damage to the surrounding areas during each LTA test (7,33). LTA was used in this study to identify the particles observed in the PFM-AFM images. It is noted that for the low drug-loaded formulations (10 and 20% w/w drug loadings), most tested points show single glass transition within the temperature range of 40–65°C (data not shown). No crystalline felodipine melting was detected for the formulations with low drug loadings. It is possible that the drug crystals with submicron dimensions were dissolved in the glassy polymer when the polymer was heated by the thermal probe. Similar effect was observed in the previous DSC studies of the extrudates (6). With increasing the drug loading (30, 50, and 70%), the results of the LTA tests of the surfaces of the samples display more variations than the low drug loading formulations. This is demonstrated by an example of a 50/50 extrudate surface. As seen in Fig. 6, multiple particles can be seen in the topography of the surface of a 50/50 extrudate. LTA was performed at four different locations observed in the topography of the sample surface. Three of these selected locations are on particulate-shaped regions, and one test point is on the flat region. Since the nanoprobe induces less thermal damage of the surrounding area, the results of the four test points should represent the original thermal behaviour of each individual point.

It can be seen in Fig. 6 that point 1 shows a softening at 85°C and a deeper tip penetration at 149°C, which is close to the melting of the crystalline felodipine form I. This indicates the particle is a felodipine crystal coated with polymer layer. This is in good agreement with the PFM-AFM results discussed previously. For points 2 and 3, although both areas show particulate appearances, the LTA results of the two points show single softening at 56°C and 66°C, respectively. Two possible explanations for the results: 1) it is possible that the particles 2 and 3 are amorphous/nano-crystalline felodipine mixed with polymer; 2) these particles are coated with a thick layer of polymer or mixture of the amorphous felodipine and

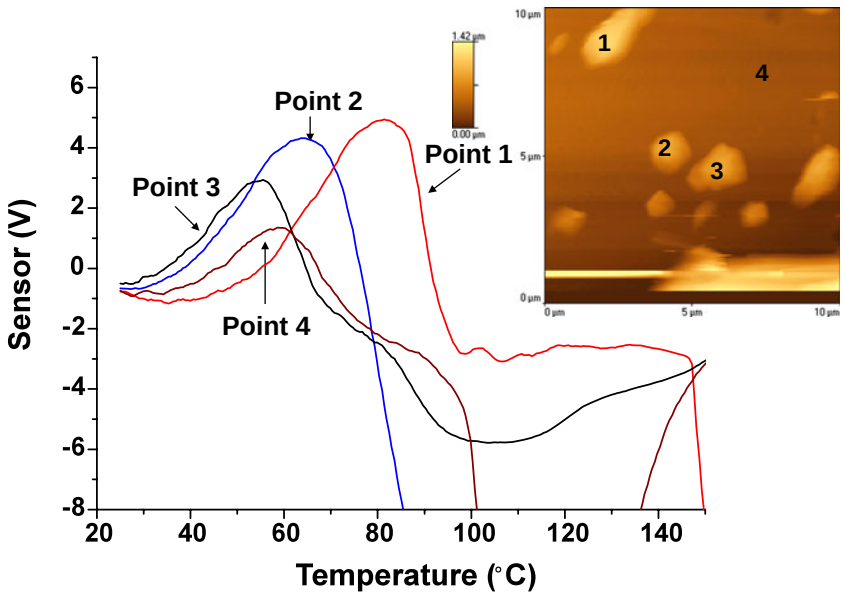

Fig. 6 LTA results of the surface of the aged 70/30 felodipine/ Eudragit® E PO HME extrudate with illustrated sampling points on the PFM-AFM images (*left-topography image; right-adhesion image*) of the sample.

polymer. Point 4 was tested in a flat region. This only shows a softening at 59°C. The LTA results confirmed the presence of crystalline felodipine in the aged 50/50 extrudates, which is not revealed by the conventional DSC, but confirmed by the ATR-FTIR and PFM-AFM studies. The findings of PFM-AFM and LTA studies agree that the appearances of particulate features have no direct correlation with the physical and chemical nature of the particles/domains. In this case, LTA has demonstrated its potential of revealing the identities of the multilayered materials.

Photothermal Fourier-Transform Infrared (PT-FTIR) Microspectroscopy Analysis of Phase Separation in the Aged HME Formulations

Photothermal spectroscopy is a technique that can detect thermal generated by the absorption of optical radiation and subsequent radiationless de-excitation directly (8). The heat generated by the absorption of the IR beam diffuses through the sample, and the measurement of the heat generated *versus* wavelength results in an infrared spectrum. PT-FTIR microspectroscopy uses this principle by testing the samples using a Wollaston thermal probe (8–10). In this study, the Wollaston thermal probe was coupled with the photothermal spectrometer to gain localised spectroscopic information of the formulations, such as chemical composition and physical forms of the components. This novel analytical technique has been increasingly used for chemical and physical identification of pharmaceutical-related materials (7–9,33). The wavelength of the energy absorption (the location of the PT peaks) of the photothermal measurements is the same as conventional IR measurements, but with slightly different relative peak intensities (9). Therefore, for the same material the peaks in the photothermal spectrum appear at the same wavenumber as its IR spectrum, while the intensities of the peaks are broader than the corresponding conventional IR spectrum. The resolution of the PT-FTIR microspectroscopy technique is dependent on the tip selection and the thermal diffusion properties of the sample. The technique is still being developed, and current estimates of the spatial resolution using the Wollaston tip on a polymeric material are 10–25 μm (34).

The surface spectra of the extrudates were first obtained using the PT-FTIR microspectroscopy with a Wollaston probe. The N-H (3340–3260 cm^{-1}) and C=O (1780–1600 cm^{-1}) regions of the spectra are shown in Fig. 7a. It can be seen that the relative intensity of the N-H peak at 3370 cm^{-1} associated with the presence of crystalline felodipine form I increases with increasing the drug loading. When the drug loading is above 30%, the 3370 cm^{-1} N-H stretching peaks display asymmetric shape and a shoulder peak is developed at around 3340 cm^{-1}. According to the ATR-FTIR results, the 3340 cm^{-1} N-H peak is associated with the presence of either amorphous felodipine or crystalline form II. Therefore, combined with MTDSC results (6) and the ATR-FTIR results, this indicates the presence of amorphous and crystalline felodipine form II in the 50 and 70% formulations. In the C=O regions, for the formulations with 10–30% drug loadings, only the 1700 cm^{-1} peak corresponding to the presence of felodipine is observed. However, the absence of the H-bonded C=O peak (1682 cm^{-1} for crystalline or 1677 cm^{-1} for amorphous felodipine) makes it difficult to conclude the physical forms of the drug in these formulations. In this case, since the ATR-FTIR results of the extrudates with low drug loadings have indicated the main physical forms of the drug is crystalline in the formulations, it is reasonable to suggest that the shoulder peak at 1682 cm^{-1} with low intensity is obscured by the 1700 cm^{-1} peak. For the formulation with 70% drug loading, the peak ratio of 1725/1700 cm^{-1} (polymer/drug) is significantly reduced. The 1700 cm^{-1} peak of the formulations has higher intensity than the 1725 cm^{-1} polymer C=O peak. A shoulder peak within the region of 1690–1670 cm^{-1} can clearly be observed. However, it is difficult to assign the peak maximum of this shoulder peak because of its breadth and the high degree of merging with the 1700 cm^{-1} peak. In order to attempt to deconvolute the peaks, we have used Gaussian fitting to the peak envelope as a rapid assessment of the positions of the peak maximum. We recognise that in practice the peaks are not Gaussian but believe that the Gaussian approximation is sufficient for the purposes of deconvolution. After deconvolution, the shoulder peaks are observed at approximately 1678 cm^{-1} (as seen in Fig. 7b). This indicates high content of amorphous felodipine on the surface of the 70/30 extrudates. This agrees well with the conclusion obtained from the N-H regions spectra of these two formulations and the ATR-FTIR results.

The PT-FTIR microspectroscopy was used to further investigate the drug distribution across the aged extrudates. The previous ATR-FTIR results of the high drug loading formulations have shown the difference in the drug concentration on the surface and at the cross-section of the formulations. The PT-FTIR spectra of the 10 different locations on the surface of the 10/90 and 30/70 extrudates are compared in Fig. 8. In the C=O region of the 10/90 HME formulation, a shoulder peak at 1700 cm^{-1} related to the non-hydrogen-bonded C=O stretching can be seen in both surface and cross-section spectra of different locations of the extrudates. Most of the spectra overlap, and no significant variation can be observed in the peak shape and intensity ratio between the peak at 1725 cm^{-1} (polymer related C=O band) and the shoulder peak at 1700 cm^{-1} (drug related C=O band) for both surface and cross-section

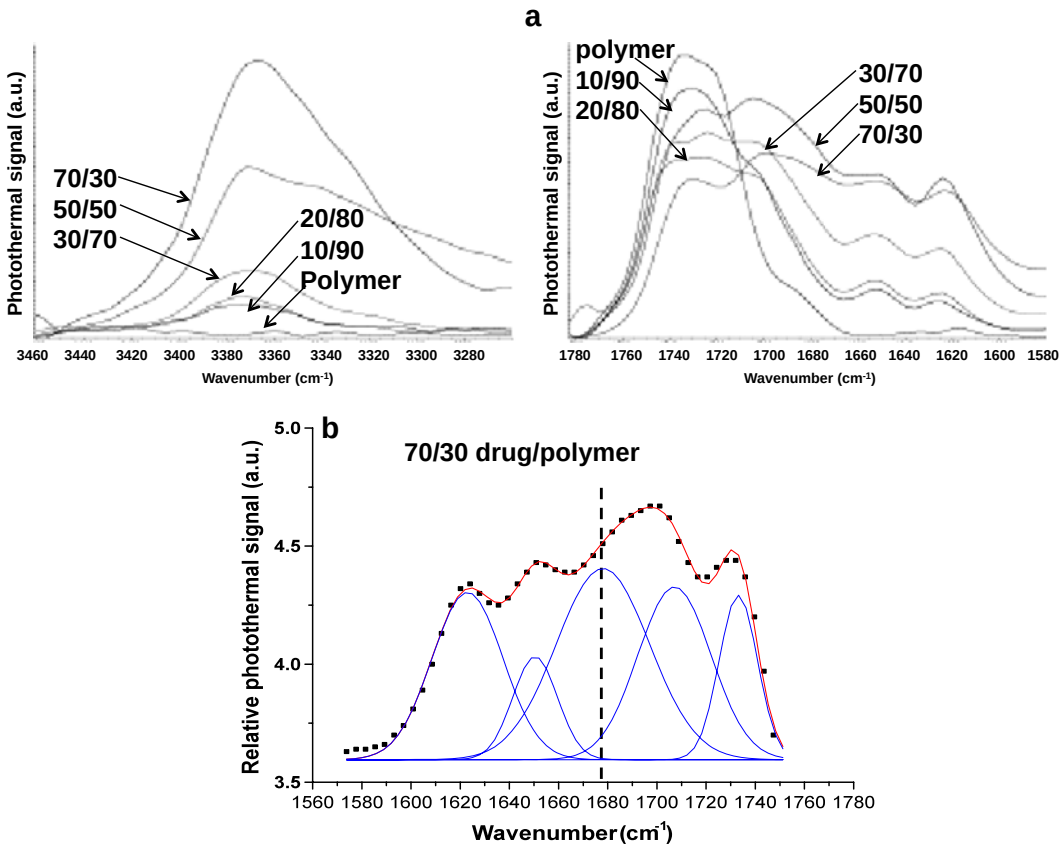

Fig. 7 PT-FTIR microspectroscopy spectra of (**a**) the surfaces of the aged HME felodipine/ Eudragit® E PO extrudates in the regions of 3440–3240 cm^{-1} and 1780–1580 cm^{-1}; (**b**) deconvolution of the surface spectra of the aged 50/50 and 70/30 HME extrudates in the region of 1780–1580 cm^{-1}.

of the extrudates. This suggests the relatively homogenous distribution of drug across the 10/90 extrudates within the testing capacity of the spatial resolution of this technique (micron range). The spectra obtained on the surface of the 30/70 extrudate reveal high variation in the ratio of the intensities of the peaks at 1725 and 1700 cm^{-1}. This

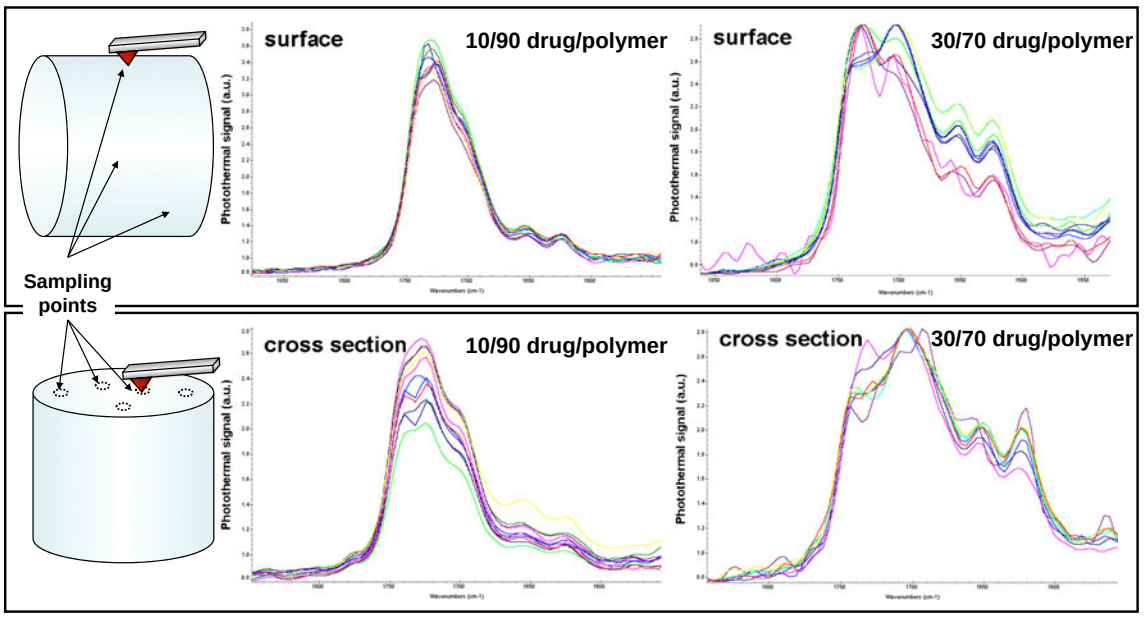

Fig. 8 PT-FTIR microspectroscopy spectra of the different sampling points on the surface (*top panel*) and the cross-section (*bottom panel*) of the aged 10/90 and 30/70 felodipine/ Eudragit® E PO extrudates.

indicates the marked difference in the drug concentration of each tested location on the surface of the extrudates. This is in good agreement with the PFM-AFM results and is not revealed by global characterisation methods, such as ATR-FTIR and DSC/MTDSC. The spectra with lower ratio between the intensities of the peaks at 1725 and 1700 cm^{-1} represent the locations with higher felodipine concentrations. The spectra of the 10 different tested locations on the cross-section of the extrudates show less variations in terms of the 1725 cm^{-1}/1700 cm^{-1} peak intensity ratio compared to the surface. However, it can be seen that the average peak intensity ratio of 1725 cm^{-1}/1700 cm^{-1} is much lower than the one of the surface. This can be explained by the higher drug concentration and lower heterogeneity in the cross-section of the 30/70 HME extrudates.

The PT-FTIR microspectroscopy study provides complementary spectroscopic information to the ATR-FTIR and LTA results on the distribution of the phase separations with micron resolution in the aged extrudates. The amorphous content of felodipine as well as the heterogeneity of drug distribution in the aged extrudates increases with increasing the drug loading. In the high drug-loaded formulations, the drug concentration is higher in the inner core than the outer layer of the aged extrudates.

DISCUSSION

The main focus of this study is to use macroscopic and localised spectroscopic and scanning probe microscopic methods to characterise the phase separation in the aged HME formulations containing felodipine with 10 to 70% drug loading. The outcome of this study has emphasised two areas in hot-melt-extruded formulation development: the complexity of the nature of the dispersion despite it being a binary system, and the advantages of localised characterisation combined with conventional analytical approaches for studying these systems.

Physical State and Distribution of Felodipine in Aged HME Formulations

The physical form of felodipine in the aged HME formulations was examined using macroscopic spectroscopic techniques (ATR-FTIR spectroscopy) as well as localised approaches, including PFM-AFM, LTA and PT-FTIR microspectroscopy. Due to the complexity of the polymorphism and the possibility of the presence of enantiomeric and racemic felodipine (14), it proved difficult to reach firm conclusions on the physical state of felodipine in the aged formulations. However, the combined characterisation approach used in this study allowed more detailed assessments on the physical state of the drug in the formulation in comparison to only using macroscopic analyses (6). As seen in Table 1, the formulations with drug loadings at or below 30% displayed evidence of the presence of crystalline form I. For the formulations with 50 and 70% drug loadings, felodipine presents as different physical forms in the centre and at the surface of the aged extrudates. For the 50% drug-loaded extrudates, mainly crystalline felodipine was identified on the surface of the samples. On the basis of the spectroscopic evidence, it is likely that the surface contains felodipine form I and II. For the aged extrudates with 70% drug loading, the surface also contains a larger amount of amorphous felodipine compared to the 50% formulations. This may be associated with a limited amount of crystallisation. As the 70% formulation has higher drug content and a higher level of supersaturation, more amorphous drug domains were separated from the molecular dispersion on aging. These amorphous domains can potentially develop into crystal drug particles over longer aging periods. Both high drug loading formulations exhibit high content of amorphous felodipine in the centre of the extrudates in comparison to their surfaces, and no crystalline felodipine was detected at the centre of the 70% formulation.

Potential Pathways of Phase Separation in the Aged HME Formulations

Phase separation can be initiated at any stage of the HME process after raw material feeding. In the liquidified stage of the HME, if a drug and a polymer are highly miscible, the drug is likely to be molecularly dispersed in the glassy polymer. If the drug and the polymer are highly immiscible, the possibility of demixing (liquid drug forming small

Table I Prediction of the Physical Forms of Felodipine in the Aged HME Formulations

Physical form of felodipine	10–30% drug loading	50% drug loading		70% drug loading	
		Surface	Cross-section	Surface	Cross-section
Prediction of the physical state of felodipine in the extrudates	Form I	Mainly Form I Form II	Mainly Form II Am	Form I Form II Am	Am

Am stands for amorphous felodipine

droplets in the molten polymer) should theoretically be high. The size of the drug droplets can be in micron or even nanometer size because of the high shear force resulting from the rotation of screws. These drug domains can further develop into the crystalline drugs during aging process. This is likely to be the case for the felodipine-Eudragit® E PO systems, since the miscibility of the drug and the polymer is relatively low (6). During the extrusion stage of the HME operation, most polymers tend to expand to some extent as a result of the significant pressure reduction, which can be partially responsible to the uneven drug distribution of the HME samples. When the polymer-drug mixture is extruded out from the die, the polymer at the outer layer carrying certain amount of the drug expands extensively, which leaves the rest of the drug concentrate in the centre. The rapid reductions in temperature and pressure of the sample may also initiate the nucleation process of the drug in the polymer. Depending on the type of nucleation, homogeneous or heterogeneous, the phase separation can be in the form of amorphous or crystalline drug domains, respectively. According to nucleation theory, a low degree of supersaturation favours heterogeneous nucleation, which often leads to crystalline formation, and exposure to foreign nucleus (such as dust particles and the particles shed from the instrument parts during processing) can also initiate crystallisation; a high degree of supersaturation tends to lead to homogeneous nucleation, which often leads to the formation of amorphous clusters (35–37). For the extrudates with high drug loadings, the difference between the surface (low drug concentration, low degree of supersaturation) and centre (high drug concentration, high degree of supersaturation) may be attributed by the different type of nucleation processes. The extrudate centre is dominated by homogeneous nucleation leading to the formation of amorphous domains, whereas the surface layer is more dominated by heterogeneous nucleation as well as more exposure to external environment such as dust particles (38) leading to crystallisation.

Strength and Weakness of the Used Analytical Techniques

The investigation into the drug distribution in the aged extrudates demonstrated that the analytical techniques used all appeared to have strengths and limitations which were largely complementary. Both ATR-FTIR spectroscopic and PT-FTIR microspectroscopic results agreed that the drug was evenly distributed in the aged extrudates with 10 and 20% drug loading and that the aged 50 and 70% drug-loaded formulations possessed a crystalline drug-rich surface and amorphous drug-rich centre. However, the ATR-FTIR spectroscopy method did not detect any difference in the drug distribution in the aged extrudates with 30% drug loading, whereas the PT-FTIR microspectroscopy revealed the higher drug content and more homogeneous drug distribution in the centre of the extrudates compared to the surfaces of the samples through localised tests. For the high drug loading (50% and 70%) formulations, the results of the global and localised characterisation approaches exhibited good agreement. Both methods provided evidence of the higher drug concentration and more amorphous felodipine content preserved in the centre than on the surface of these aged extrudates. PFM-AFM and LTA facilitated the identification of phase separation in the extrudates locally with the resolution on a micron to submicron scale, which cannot be achieved by conventional macroscopic methods. Although it could be argued that confocal Raman microscopy can achieve similar resolution, Raman spectroscopy often struggles when samples/drugs such as felodipine fluoresce. A drawback of the use of localised analytical techniques is that high numbers of repeated tests are required in order to obtain representative results. This can be time consuming in comparison to conventional macroscopic methods. In summary, the localised methods are highly desirable for locating and identifying low quantity phase separations with micron to submicron dimensions. For the samples in which localised information of the samples (i.e. drug/polymer domains distributions) significantly aids understanding formulation *in vitro*/*in vivo* performance, localised analytical tools can provide complementary knowledge to that gained by use of conventional macroscopic instrumentation.

CONCLUSION

Hot-melt-extruded felodipine and Eudragit® E PO systems were studied after aging. It was noted that crystalline felodipine presents in all formulations with drug loadings from 10–70% (w/w). In the formulations with high drug loadings (50 and 70%), amorphous felodipine co-exists with the crystalline form and is concentrated in the centre of the extrudates. The combined use of the ATR-FTIR, PFM-AFM, and LTA and PT-FTIR microspectroscopy indicated that the uneven drug distribution in the formulations with higher drug loadings (in particular the surface layer of the extrudates) and the drug crystals in the extrudates with low drug loadings are small in size, likely to be nanocrystals. We proposed that uneven drug distribution is mainly caused by the expansion of the extrudates during extrusion. The variation in the amorphous drug contents in the formulations with different drug loading is likely associated with their difference in the degree of supersaturation of the drug

in these formulations, which leads to different nucleation pathways.

ACKNOWLEDGMENTS

The authors would like to thank Dr. Jonathon Moffat and Prof. Mike Reading for their assistance on the use of PT-FTIR microspectroscopy.

REFERENCES

1. Breitenbach J. Melt extrusion: from process to drug delivery technology. Euro J Pharm Biopharm. 2002;54(2):107–17.
2. Miller DA, McConville JT, Yang W, Williams III RO, McGinity JW. Hot-melt extrusion for enhanced delivery of drug particles. J Pharm Sci. 2006;96(2):361–76.
3. Crowley MM, Zhang F, Repka MA, Thumma S, Upadhye SB, Battu SK, *et al.* Pharmaceutical applications of hot-melt extrusion: part I. Drug Dev Ind Pharm. 2007;33(9):909–26.
4. Mackellar AJ, Buckton G, Newton JM, Chowdhry BZ, Orr CA. The controlled crystallisation of a model powder: 1. The effects of altering the stirring rate and the supersaturation profile, and the incorporation of a surfactant (poloxamer 188). Int J Pharm. 1994;112(1):65–78.
5. Laarhoven JAH, Kruft MAB, Vromans H. Effect of supersaturation and crystallization phenomena on the release properties of a controlled release device based on EVA copolymer. J Control Release. 2002;82(2–3):309–17.
6. Qi S, Belton P, Nollenberger K, Clayden N, Reading M, Craig DQM. Novel characterisation of phase separation in hot melt extruded solid dispersions: a thermal, microscopic and NMR relaxometry study. Pharm Res. 2010;27:1869–83.
7. Harding L, Qi S, Hill G, Reading M, Craig DQM. The development of microthermal analysis and photothermal microspectroscopy as novel approaches to drug–excipient compatibility studies. Int J Pharm. 2008;354(1–2):149–57.
8. Dai X, Moffat JG, Mayes AG, Reading M, Craig DQM, Belton PS, *et al.* Thermal probe based analytical microscopy: thermal analysis and photothermal fourier-transform infrared microspectroscopy together with thermally assisted nanosampling coupled with capillary electrophoresis. Analy Chem. 2009;81(16):6612–9.
9. Moffat JG, Mayes AG, Belton PS, Craig DQM, Reading M. Compositional analysis of metal chelating materials using near-field photothermal fourier transform infrared microspectroscopy. Analy Chem. 2010;82(1):91–7.
10. Qi S, Gryczke A, Belton P, Craig DQM. Characterisation of solid dispersions of paracetamol and EUDRAGIT® E prepared by hot-melt extrusion using thermal, microthermal and spectroscopic analysis. Int J Pharm. 2008;354(1–2):158–67.
11. Hammiche A, Bozec L, Pollock HM, German M, Reading M. Progress in near-field photothermal Infra-red microspectroscopy. J Microscopy. 2004;213(2):129–34.
12. Lou B, Boström D, Velaga SP. Polymorph control of felodipine form II in an attempted cocrystallization. Cryst Growth Des. 2009;9(3):1253–7.
13. Knoon H, Taylor LS. Influence of different polymers on the crystallization tendency of molecularly dispersed amorphous felodipine. J Pharm Sci. 2006;95(12):2692–705.
14. Rollinger JM, Burger A. Polymorphism of racemic felodipine and the unusual series of solid solutions in the binary system of its enantiomers. J Pharm Sci. 2001;90(7):949–59.
15. Tang XC, Pikal MJ, Taylor LS. A spectroscopic investigation of hydrogen bond patterns in crystalline and amorphous phases in dihydropyridine calcium channel blockers. Pharm Res. 2002;19(4):477–83.
16. Chamarthy SP, Pinal R. The nature of crystal disorder in milled pharmaceutical materials. Colloid Surface A. 2008;331(1–2):68–75.
17. Feng T, Carvajal MT, Pinal R. Process induced disorder in crystalline materials: differentiating defective crystals from the amorphous form of Griseofulvin. J Pharm Sc. 2008;97:3207–21.
18. Wildfong PLD, Hancock BC, Moore MD, Morri KR. Towards an understanding of the structurally based potential for mechanically activated disordering of small molecule organic crystals. J Pharm Sci. 2006;95:2645–56.
19. Bates S, Zografi G, Engers D, Morris K, Crowley K, Newman A. Analysis of amorphous and nanocrystalline solids from their X-ray diffraction patterns. Pharm Res. 2006;23:2333–49.
20. Rumondor A, Stanford L, Taylor L. Effects of polymer type and storage relative humidity on the kinetics of felodipine crystallization from amorphous solid dispersions. Pharm Res. 2009;26(12):2599–606.
21. Tang XC, Pikal MJ, Taylor LS. A spectroscopic investigation of hydrogen bond patterns in crystalline and amorphous phases in dihydropyridine calcium channel blockers. Pharm Res. 2002;19(4):447–83.
22. Vasanthavada M, Tong WQ, Joshi Y, Kislalioglu MS. Phase behaviour of amorphous molecular dispersions II: role of hydrogen bonding in solid solubility and phase separation kinetics. Pharm Res. 2004;22(3):440–8.
23. Rosa-Zeiser A, Weilandt E, Weilandt H, Marti O. The simultaneous measurement of elastic, electrostatic and adhesive properties by scanning force microscopy: pulsed-force mode operation. Meas Sci Technol. 1997;8(11):1333–8.
24. Marti O, Stifter T, Waschipky H, Quintus M, Hild S. Scanning probe microscopy of heterogeneous polymers, colloids surf. A. 1999;154(1–2):65–73.
25. Krotil HU, Stifter T, Waschipky H, Weishaupt K, Hild S, Marti O. Pulsed force mode: a new method for the investigation of surface properties. Surf Interface Anal. 1999;27:336–40.
26. Miyatani T, Okamoto S, Rosa A, Marti O, Fujihira M. Surface charge mapping of solid surfaces in water by pulsed-force-mode atomic force microscopy. Appl Phys A. 1998;66:S349–52.
27. Miyatani T, Horii M, Rosa A, Fujihira M, Marti O. Mapping of electrical double-layer force between tip and sample surfaces in water with pulsed-force-mode atomic force microscopy. O Appl Phys Lett. 1997;71:2632–4.
28. Rezende CA, Lee LT, Galembeck F. Surface mechanical properties of thin polymer films investigated by AFM in pulsed force mode. Langmuir. 2009;25(17):9938–46.
29. Grandy DB, Hourston DJ, Price DM, Reading M, Silva GG, Song M, *et al.* Microthermal characterization of segmented polyurethane elastomers and a polystyrene-poly(methyl methacrylate) polymer blend using variable-temperature pulsed force mode atomic force microscopy. Macromolecules. 2000;33(25):9348–59.
30. Zhang H, Mullen K, De Feyter S. Pulsed-force-mode AFM studies of polyphenylene dendrimers on self-assembled monolayers. J Phys Chem C. 2007;111(23):8142–4.
31. Deng KQ, Winnik MA, Yang N, Jiang ZH, Yaneff PV, Ryntz RA. Characterizing interfacial structure of TPO/CPO/TPO adhesive joints by PFM-AFM and SEM. Polymer. 2009;50(14):3225–33.

32. Zhu M, Akari S, Mohwald H. Detection of single PSS polymers on rough surface by pulsed-force-mode scanning force microscopy. Nanoletters. 2001;1:569–73.
33. Dai X, Reading M, Craig DQM. Mapping amorphous material on a partially crystalline surface: nanothermal analysis for simultaneous characterisation and imaging of lactose compacts. J Pharm Sci. 2009;98(4):1499–510.
34. Hammiche A, Bozec L, Pollock HM, German M, Reading M. Progress in near-field photothermal infra-red microspectroscopy. J Microscopy. 2004;213(2):129–34.
35. Boskey AL, Posner AS. Formation of hydroxyapatite at low supersaturation. J Phys Chem. 1976;80(1):40–5.
36. Schlomach J, Quarch K, Kind M. Investigation of precipitation of calcium carbonate at high supersaturations. Chem Eng Technol. 2006;29(2):215–20.
37. Mullin JM. Crystallization. 4th ed. Oxford: Elsevier Butterworth-Heinemann; 2001.
38. Bruce C, Fegely KA, Rajabi-Siahboomi AR, McGinity JW. Crystal growth formation in melt extrudates. Int J Pharm. 2007;341(1–2):162–72.